APME — Actualităţi şi Perspective în Domeniul Maşinilor Electrice
Electric Machines, Materials and Drives - Present and Trends
21, *1*, pp. 54-63, 2025

ANALYSIS OF THE ASYNCRONOUS MOTOR IN STEADY-STATE REGIME WHEN TAKING INTO CONSIDERATION THE MAGNETIZATION CHARACTERISTIC AND THE VARIATION OF THE ROTOR RESISTANCE WITH SLIP

Mihai ROTARU[1],Adrian-Florian GEORGESCU[1],Mihai IORDACHE[1], Dragoș NICULAE[1], Steliana PUȘCAȘU[1], Georgiana ZAINEA[1].
[1]Dept. of Electrical Engineering, Faculty of Electrical Engineering, National University of Science and Engineering Politehnica of Bucharest,
mihai.rotaru2002@stud.electro.upb.ro, adrian.georgescu72@stud.electro.upb.ro, mihai.iordache@upb.ro, dragos.niculae@upb.ro, steliana.puscasu@upb.ro, georgiana.zainea@upb.ro

Abstract: In this paper, the influence of saturation on the performance of asynchronous motors is studied. To this end, starting from the equivalent scheme, we take into account that the film–iLm characteristic is treated as a current-controlled nonlinear inductor, and the rotor resistor on a phase is modeled as a time-variable resistor; the asynchronous motor operating in steady-state behavior was analyzed. The simulations were done by the dedicated performance programs (elaborated by the authors): ACAP – Analog Circuit Analysis Program, CSAP – Circuit Symbolic Analysis Program, and, to compare the results, by the SPICE program. All these programs are based on the modified nodal equations and permit Fourier analysis of all current and voltage waveforms. Thus, we can compute any higher-order harmonics that appear in the time variations of these quantities. Analyzing the results, we conclude that, due to high-order harmonics in the current variations, losses increase and, consequently, the asynchronous motor's performance decreases (e.g., efficiency and power factor). The analysis of the saturation effect on an asynchronous motor in steady-state behavior can also be performed using the state equations, which can be integrated with one of the MATLAB integration routines.

1. INTRODUCTION

The study of the non-sinusoidal periodic regime is important both from the point of view of the disturbing effects produced in the transmission and distribution networks of electric energy, and from that of its use in the construction of some electrical devices. In electrical networks that operate in a non-sinusoidal periodic behavior - also called a deforming regime, the power factor decreases, compensation of reactive power with capacitors is generally not possible, additional energy losses occur, resonances occur (which produce over voltages or over currents) etc. The nonlinearity of some circuit elements - saturated iron-core coils, nonlinear capacitors - is used in the construction of electrical devices such as: magnetic amplifiers, ferromagnetic voltage stabilizers, frequency multipliers etc.

In recent years, numerous analysis methods have been developed for autonomous and non-autonomous circuits, in order to determine the response in the steady-state behavior. These methods can be organized into two classes:

- Methods based on time-domain analysis;
- Methods based on frequency-domain analysis.

The first class represents different variants of the "well-known Shooting Method (SH)" and the second one the methods represent the different variants of the harmonic balance method (HBM) [1 – 3, 10 – 18].

ISSN / ISSN-L: 1843-5912
DOI: 10.36801/apme.2025.1.6

Analyzing the equivalent circuit of the induction motor, using the state equations and/or the modified nodal equations, till when it obtained the steady-state behavior – the shooting method, [4 – 18].

The simulations can be done by the dedicated performance programs (elaborated by the authors): ACAP – Analog Circuit Analysis Program [6], CSAP – Circuit Symbolic Analysis Program and TFSYG – Transfer Function Symbolic Generation [5] and, for to compare the results, by the SPICE [3] (in this case the rotor resistance is considered constant equal to *R'r/an* – *an* is the nominal slip.When the SPICE program is used to simulate electrical circuits with current-controlled nonlinear circuit elements, the models presented in [3] are used.

To illustrate the effects produced by the presence of nonlinear and/or time variable circuit elements, the analysis of the asynchronous motor is considered when taking into account the magnetization characteristic and the *R'r/a* - time characteristic (in fact, *R'r/a* is a time variable circuit element function of the slip) and the ACAP and MATLAB programs.

It was found out an excellent correspondence between the asynchronous motor ratings obtained through simulation with the catalog data. When take into account saturation phenomenon, the phase current displays high order harmonics. An immediate consequence of the presence of these current harmonics was an increase in the losses and a decrease of the efficiency and the motor power factor in comparison to the non-saturated magnetic core assumption. In Section II is described the simulation of the asynchronous motor in steady-state behavior. Some conclusions are presented in Section III.

2. SIMULATION OF THE ASYNCHRONOUS MOTOR IN THE STEADY-STATE BEHAVIOR

We consider the equivalent circuit of the induction motor shown in figure 1, [4].

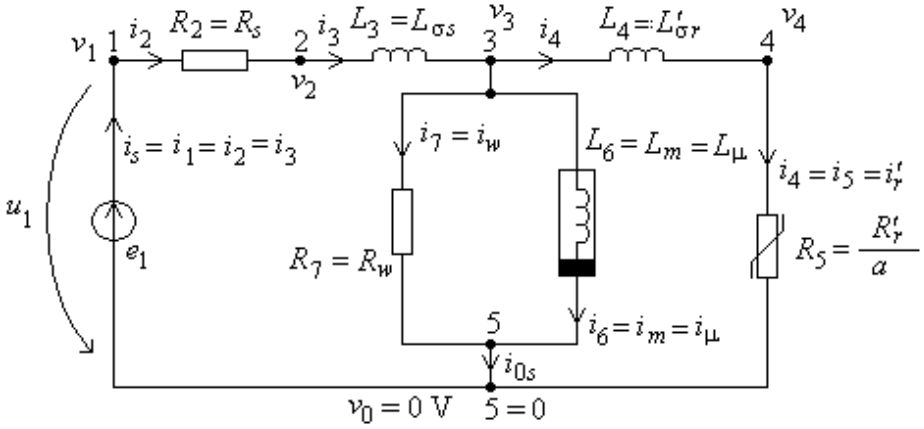

Fig.1 – Asynchronous motor equivalent scheme.

The circuit in Fig. 1 contains a current-controlled nonlinear inductor L_6 with the nonlinear characteristic (Fig. 2) and a time-variable resistor , a being the slip (Fig. 3).

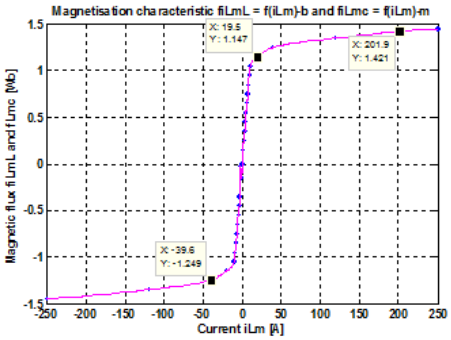

Fig. 2 – Magnetization nonlinear characteristic $\boldsymbol{\phi_{L6} = \hat{\phi}_{L6}(i_6)}$

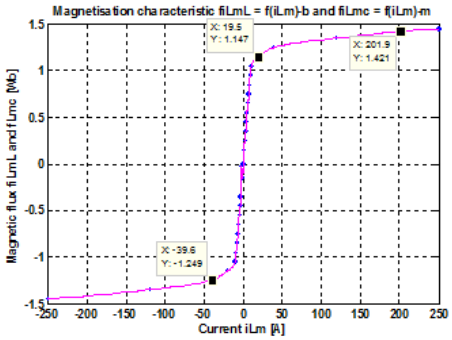

Fig. 3 – The characteristic of the time-variable resistor R5.

The state equations in the symbolic–normal form for the induction motor (fig. 1) have the following form:

$$\frac{d}{dt}\begin{bmatrix} i_3 \\ i_4 \\ i_6 \end{bmatrix} = \begin{bmatrix} -\dfrac{R_2+R_7}{L_3} & \dfrac{R_7}{L_2} & \dfrac{R_7}{L_2} \\ \dfrac{R_7}{L_4} & -\dfrac{R_7+R_{p5}}{L_4} & -\dfrac{R_7}{L_4} \\ \dfrac{R_7}{L_{di6}(i_6)} & -\dfrac{R_7}{L_{di6}(i_6)} & -\dfrac{R_7}{L_{di6}(i_6)} \end{bmatrix} \cdot \begin{bmatrix} i_3 \\ i_4 \\ i_6 \end{bmatrix} + \begin{bmatrix} \dfrac{1}{L_3} \\ 0 \\ 0 \end{bmatrix} \cdot [e_1] \tag{1}$$

where the L_{di6} differential inductance has the espression $\boldsymbol{L_{di6}(i_6) = \frac{\partial \phi_{L6}}{\partial i_6}}$.

In order to integrate the state equations (1) we can use any integration routines from the MATLAB Toolboxes.

The modified nodal equations, when we use the implicit integration Euler algorithm, for the circuit in figure have the following expressions, [3]:

$$\begin{aligned}
&(n_1):\ G_2 v_{1,j+1}^{(k+1)} - G_2 v_{2,j+1}^{(k+1)} - i_{1,j+1}^{(k+1)} = 0,\\
&(n_2):\ -G_2 v_{1,j+1}^{(k+1)} + \left(G_2 + \frac{h}{L_3}\right) v_{2,j+1}^{(k+1)} - \frac{h}{L_3} v_{3,j+1}^{(k+1)} = -i_{3,j},\\
&(n_3):\ -\frac{h}{L_3} v_{2,j+1}^{(k+1)} + \left(\frac{h}{L_3} + \frac{h}{L_4} + G_7\right) v_{3,j+1}^{(k+1)} - \frac{h}{L_4} v_{4,j+1}^{(k+1)} + i_{6,j+1}^{(k+1)} = i_{3,j} - i_{4,j},\\
&(n_4):\ -\frac{h}{L_4} v_{3j+1}^{(k+1)} + \left(\frac{h}{L_4} + G_{p5}\right) v_{4,j+1}^{(k+1)} = i_{4,j}^{(\ )},\\
&(b_1):\ -v_{1,j+1}^{(k+1)} = -e_{1,(j+1)},\\
&(b_6):\ v_{3,j+1}^{(k+1)} - \frac{L_{di6}\left(s_{j+1}^{(k)}\right)}{h} i_{6,j+1}^{(k+1)} = \frac{\Phi_{L6}\left(s_{j+1}^{(k)}\right)}{h} - \frac{L_{di6}(s_j)}{h} \cdot i_{6,j} - \frac{\Phi_{L6,j}}{h},
\end{aligned} \tag{2}$$

where the independent variable vector at the time moment tj+1 = tj +h (h is the time step) and at the (k+1)th iteration has the following form:

$$x_{j+1}^{(k+1)} = \left[v_{1,j+1}^{(k+1)}\ v_{2,j+1}^{(k+1)}\ v_{3,j+1}^{(k+1)}\ v_{4,j+1}^{(k+1)}\ i_{1,j+1}^{(k+1)}\ i_{6,j+1}^{(k+1)}\right]^t \tag{3}$$

In the Eq. (2) the magnetization characteristic $\boldsymbol{\phi_{L6} = \hat{\phi}_{L6}(i_6)}$, at the time moment $\boldsymbol{t_{j+1} = t_j + h}$ (h is the time step) and at the $\boldsymbol{(k+1)^{th}}$ iteration, is piecewise linear approximated by the relation:

$$\phi_{L6,j+1}^{(k+1)} = L_{di6}\left(s_{j+1}^{(k)}\right) \cdot i_{6,j+1}^{(k+1)} + \Phi_{L6}\left(s_{j+1}^{(k)}\right). \tag{4}$$

In the relation (4) is the segment from the time moment $\boldsymbol{t_{j+1} = t_j + h}$ and from the $\boldsymbol{(k)^{th}}$ iteration, [3].

The Joule losses P_{Cu1} and P_{Cu2}, the iron losses P_{RFe}, the mechanical power P_{mec} and the electromagnetic torque M_{em} are calculated, for iteration $(\boldsymbol{k})^{\boldsymbol{th}}$, for both the linear and nonlinear cases, with the following relations, [10 – 18]:

$$\boldsymbol{P_{Cu1\_lin} = 3.0 \cdot 0.053 \cdot \left(i_{As\_lin}(k)\right)^2} \text{ and } \boldsymbol{P_{Cu1\_nel} = 3.0 \cdot 0.053 \cdot \left(i_{As\_nel}(k)\right)^2}; \quad (5, a)$$

$$\boldsymbol{P_{Cu2\_lin} = 3.0 \cdot 0.053 \cdot \left(i_{ar\_lin}(k)\right)^2} \text{ and } \boldsymbol{P_{Cu2\_nel} = 3.0 \cdot 0.053 \cdot \left(i_{ar\_nel}(k)\right)^2}; \quad (5, b)$$

$$\boldsymbol{P_{RFe\_lin} = 3.0 \cdot 200.0 \cdot \left(i_{RFe\_lin}(k)\right)^2} \text{ and } \boldsymbol{P_{RFe\_nel} = 3.0 \cdot 200.0 \cdot \left(i_{RFe\_nel}(k)\right)^2}; \quad (5, c)$$

$$\boldsymbol{P_{mec\_lin} = 3.0 \cdot 0.0657 \cdot (1.0 - 0.026)\left(i_{ar\_lin}(k)\right)^2} /0.026 \text{ and} \quad (5, d)$$

$$\boldsymbol{P_{mec\_nel} = 3.0 \cdot 0.0657 \cdot (1.0 - 0.026)\left(i_{ar\_nel}(k)\right)^2} /0.026;$$

$$\boldsymbol{M_{em\_lin} = P_{mec\_lin}(k)/\left((1.0 - 0.026) \cdot 6.28 \cdot 20.0\right)} \text{ and} \quad (5, e)$$

$$\boldsymbol{M_{em\_nel} = P_{mec\_nel}(k)/\left((1.0 - 0.026) \cdot 6.28 \cdot 20.0\right)}.$$

Using the shooting method, the paper presents the analysis of the asynchronous motor in steady state behavior. The equivalent circuit on one phase of the motor is considered, when taking into account the saturation phenomenon (the magnetizing coil *Lm* is considered nonlinear controlled in current (c.c.), Fig. 2 and the fact that the rotor resistance $\boldsymbol{R}_5 = R_{p5} = R'_{r/a}$ varies with the slip a, so it is a time variable circuit element Fig. 3.

The analysis of the equivalent circuit on one phase of the motor will be analyzed, in the time domain, using the dedicated performance programs described above, [3 – 10].

All programs also allow the Fourier analysis of the waveforms of the currents and voltages of the sides, which allows highlighting all the higher-order harmonics that appear in the time variations of these quantities.

3. Results obtained by simulations

We have considered an asynchronous motor designed for traction purposes (MABT-2). This induction motor has the following nominal parameters: P_n=100 kW; U_n=560 V; U_{fn}=323.32 V; I_{fn}=I_n = 130 A; n_1 = 1000 rpm, n= 974 rpm - n_1 (n) is the synchronous revolving speed; $fn = f1$ = 50 Hz ; p = 3; Rs = 0.053 Ω ; =0.0657 Ω ; $Ls\sigma$ = 1.034 mH; ' $Lr\sigma$ = 0.955 mH ; Lm =28.1 mH; η = 89.7%; ; $mp = Mp/Mn$=1.1; $mm = Mm/Mn$=1.8 and V. Stator windings have a *Y* connection. The magnetizing nonlinear characteristic was derived experimentally (Fig. 2). The characteristic of the time-variable resistor R_r is also given by points as function of time (Fig.3). When running the simulation using the ACAP program, we obtained the results shown in Figs. 4 – 21.

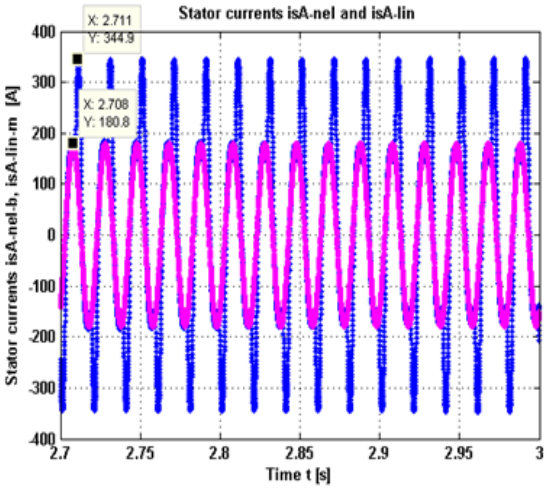

Fig. 4 – $\boldsymbol{i_{sA}}$ stator current vs time, magenta–linear, blue– nonlinear.

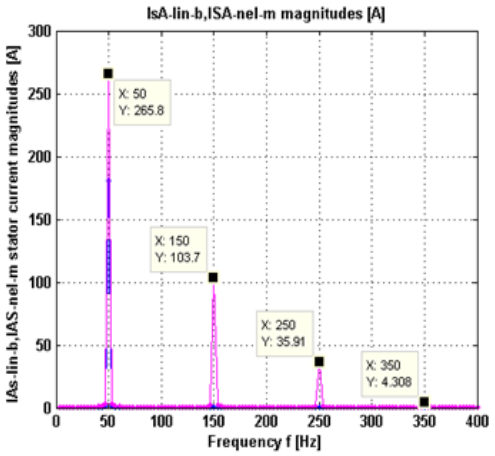

Fig.5 – $\boldsymbol{I_{sA}}$ stator current magnitude vs. frequency, blue–linear, magenta- nonlinear.

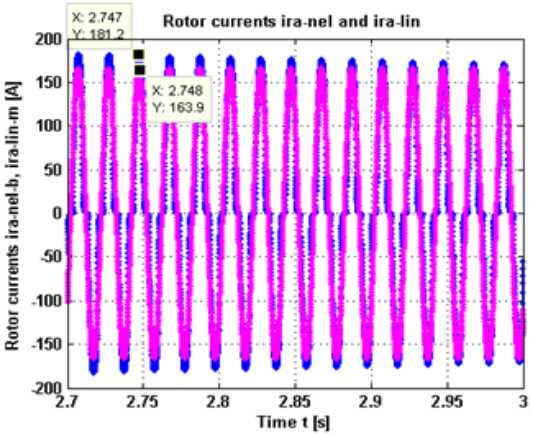

Fig.6 – $\boldsymbol{i_{ra}}$ rotor current vs time, magenta–linear, blue– nonlinear.

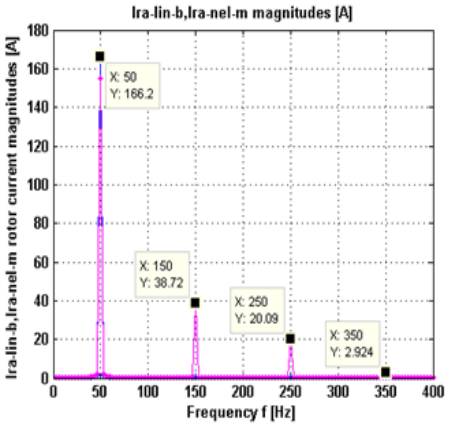

Fig.7 – $\boldsymbol{I_{ra}}$ rotor current magnitude vs. frequency, blue–linear, magenta - nonlinear.

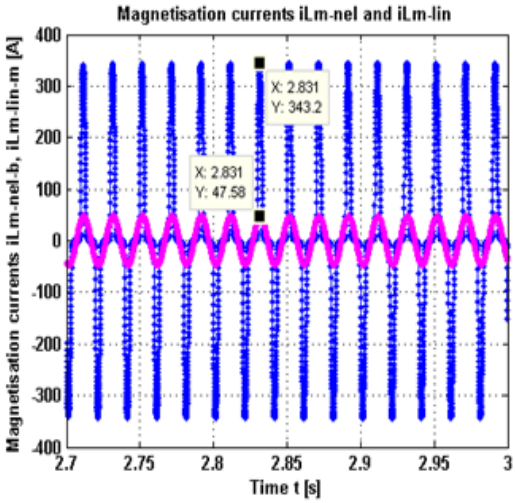

Fig.8 – $\boldsymbol{i_{Lm}}$ magnetization current vs time, magenta-linear, blue - nonlinear.

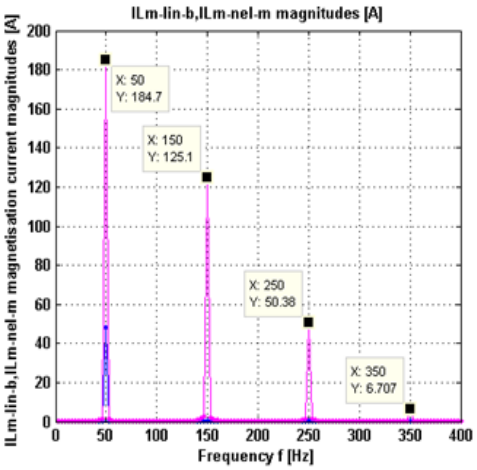

Fig. 9 – $\boldsymbol{I_{Lm}}$ magnetization current magnitude vs. frequency, blue–linear, magenta - nonlinear.

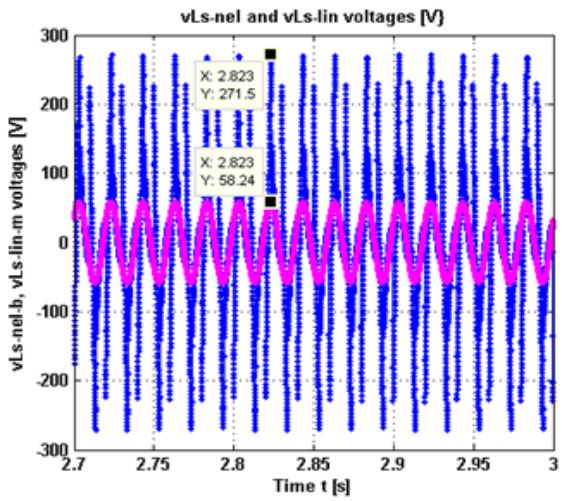

Fig.10 – $\boldsymbol{v_{Ls}}$ stator inductance voltage vs time, magenta-linear, blue - nonlinear.

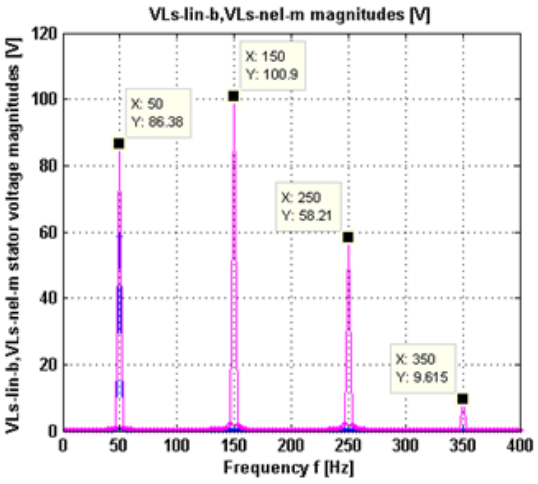

Fig.11 – $\boldsymbol{V_{Ls}}$ stator inductance voltage magnitude $\boldsymbol{V_{Ls}}$ vs. frequency, blue–linear, magenta - nonlinear.

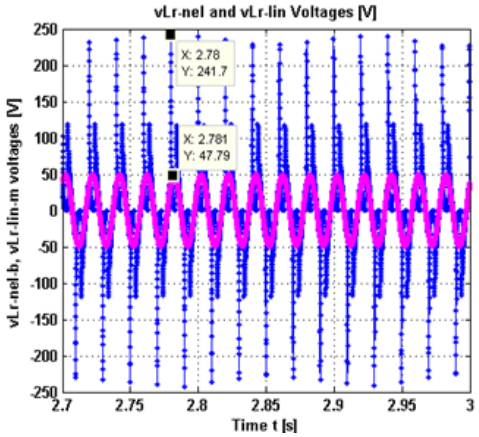

Fig. 12 – $\boldsymbol{v_{Lr}}$ rotor inductance voltage vLr vs time, magenta-linear, blue - nonlinear.

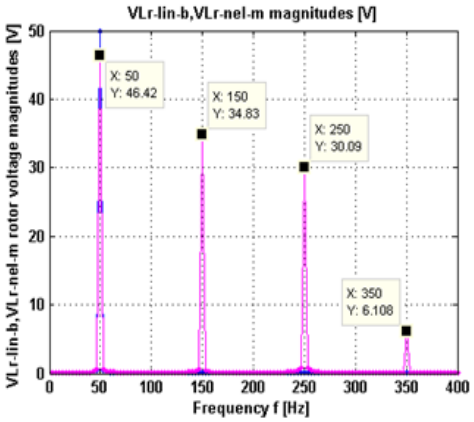

Fig. 13 – $\boldsymbol{V_{Ls}}$ rotor inductance voltage magnitude $\boldsymbol{V_{Ls}}$ vs. frequency, blue–linear, magenta - nonlinear.

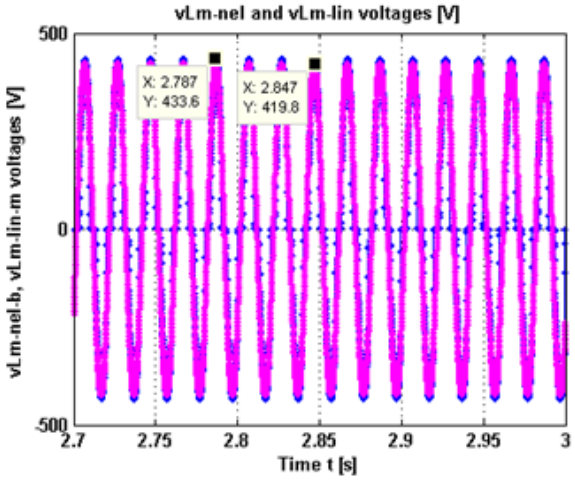

Fig. 14 – $\boldsymbol{v_{Lm}}$ magnetization inductance voltage vs time, magenta-linear, blue - nonlinear

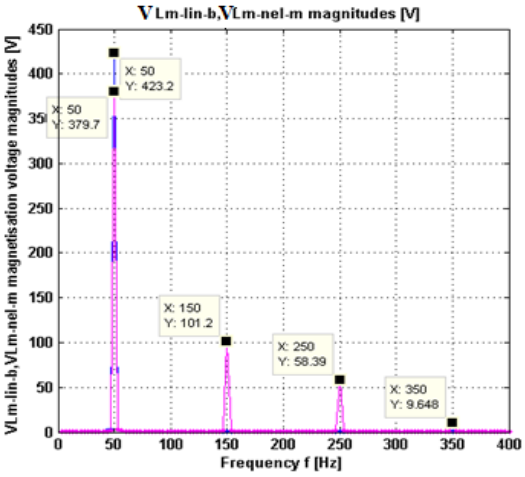

Fig. 15 – $\boldsymbol{V_{Lm}}$ magnetization inductance voltage vs. frequency, blue–linear, magenta - nonlinear.

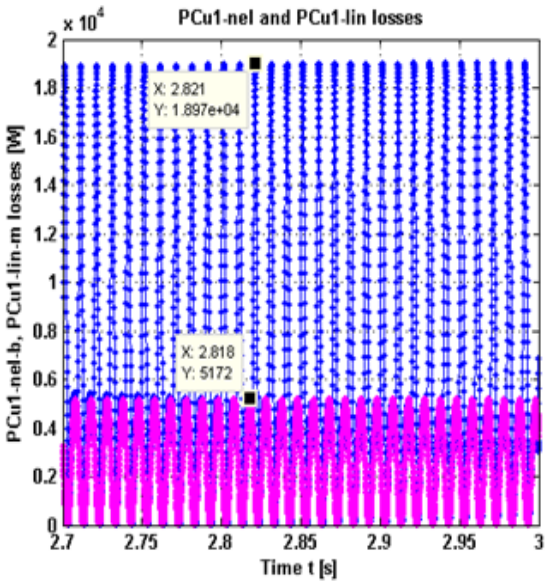

Fig. 16 – $\boldsymbol{P_{Cu1}}$ Joule's losses vs time, magenta-linear, blue - nonlinear.

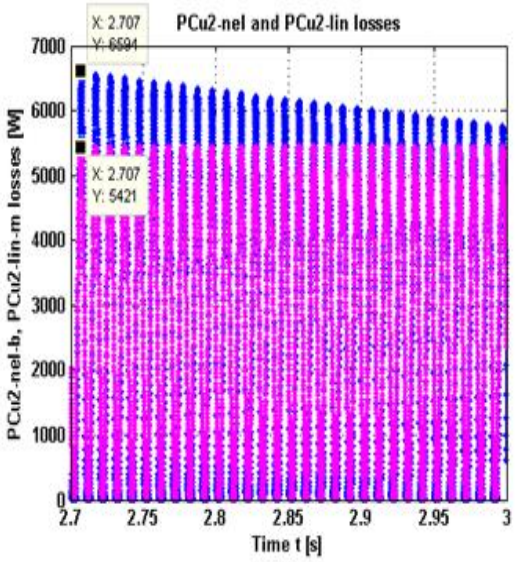

Fig. 17 – $\boldsymbol{P_{Cu2}}$ Joule's losses vs time, magenta – linear, blue – nonlinear.

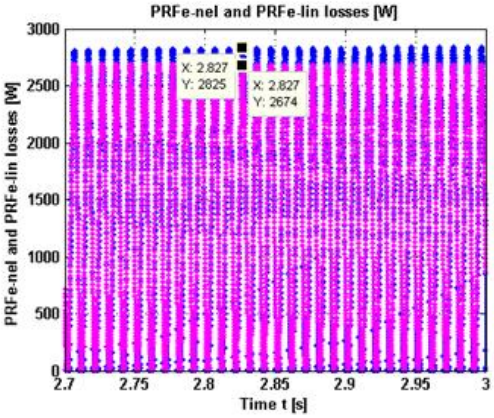

Fig. 18 – P_{RFe} iron losses vs time, magenta – linear, blue – nonlinear.

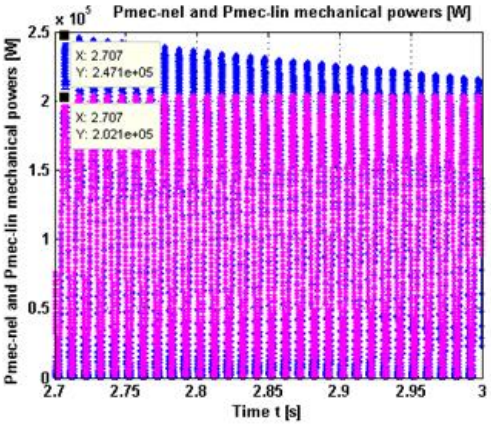

Fig. 19 – P_{mec} Mechanic power vs time, magenta – linear, blue – nonlinear.

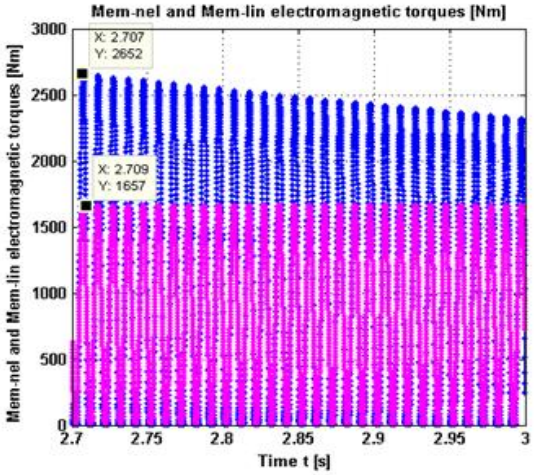

Fig. 20 – $\boldsymbol{M_{em}}$ electromagnetic torque vs time, magenta – linear, blue – nonlinear.

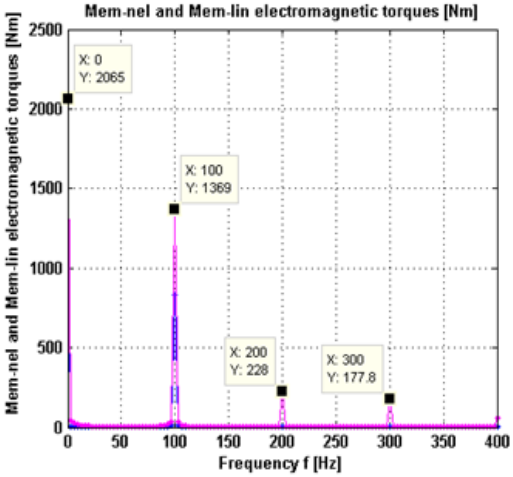

Fig. 21 – $\boldsymbol{M_{em}}$ electromagnetic torque magnitude vs. frequency, magenta–nonlinear, blue–linear.

The average losses, output power and torque are exposed in table 1 (full starting process) and table 2 (steady state behavior).

Table 1

Starting process

Quantity	Value	Unit
Average Stator Copper Loss (linear) $P_{Cu1\_ae\_lin}$	41.075	kW
Average Stator Copper Loss (nonlinear) $P_{Cu1\_ave\_nel}$	46.86	kW
Average Rotor Copper Loss (linear) $P_{Cu2\_ave\_lin}$	47.188	kW
Average Rotor Copper Loss (nonlinear) $P_{Cu2\_ave\_nel}$	38.556	kW
Average Core loss (linear) $P_{Fe\_ave\_lin}$	0.4205	kW
Average Core loss (nonlinear) $P_{Fe\_ave\_nel}$	0.413	kW
Output (Shaft) Power (linear) $P_{out\_ave\_lin}$	1767.7	kW
Output (Shaft) Power (nonlinear) $P_{out\_ave\_nel}$	15.54	kW
Electromagnetic Torque (linear) $M_{em\_ave\_lin}$	1.446×10^4	Nm
Electromagnetic Torque (nonlinear) $M_{em\_ave\_nel}$	1.554×10^3	Nm

The results in Table 1 represent the calculated values of Joule and iron losses, output power and electromagnetic torque following a motor starting process, supplied at nominal voltage and maximum load. In Table 2, the same characteristics are evaluated once the starting process has been overcome and the asynchronous motor is operating under steady-state conditions. From Tables 1 and 2 it is found that both in transient and steady-state conditions the values obtained for the linear motor and the nonlinear motor model, the values of Joule losses in copper are higher in the case of the nonlinear asynchronous motor. However, the nonlinear motor produces a higher torque. The iron losses in the magnetic core are quite similar.

Table 2

Induction motor steady state behaviour

Quantity	Value	Unit
Average Stator Copper Loss (linear) $P_{Cu1\_ave\_lin}$	2.593	kW
Average Stator Copper Loss (nonlinear) $P_{Cu1\_ave\_nel}$	6.594	kW
Average Rotor Copper Loss (linear) $P_{Cu2\_ave\_lin}$	2.5615	kW
Average Rotor Copper Loss (nonlinear) $P_{Cu2\_ave\_nel}$	2.722	kW
Average Core loss (linear) $P_{Fe\_ave\_lin}$	1.343	kW
Average Core loss (nonlinear) $P_{Fe\_ave\_nel}$	1.202	kW
Output (Shaft) Power (linear) $P_{out\_ave\_lin}$	101.964	kW
Output (Shaft) Power (nonlinear) $P_{out\_ave\_nel}$	95.961	kW
Electromagnetic Torque (linear) $M_{em\_ave\_lin}$	833.485	Nm
Electromagnetic Torque (nonlinear) $M_{em\_ave\_nel}$	1032.461	Nm

The most important harmonics (k=3,5,7) are given below in percent of the fundamental harmonic for the currents and voltages of which waveforms are displayed in the Figs. 5, 7, 9, 11, 13, 15 and 21 (see Table 3).

Table 3

Voltage and current harmonics for saturated model

Quantity	$k = 3$	$k = 5$	$k = 7$
Stator Current i_{Ask} [%]	39.01 %	13.51 %	1.621 %
Rotor Current i_{ark} [%]	23.30 %	12.09 %	1.758 %
Magnetization Current i_{Lmk} [%]	67.73 %	27.28 %	3.631 %
Stator Inductance Voltage v_{Lsk} [%]	116.8 %	67.39 %	11.12 %
Rotor Inductance Voltage v_{Lrk} [%]	75.03 %	64.82 %	13.16 %
Magnetization Inductance Voltage v_{Lmk} [%]	23.91 %	13.80 %	2.28 %

The electromagnetic torque calculated for linear model of the asynchronous motor is equal to the nominal torque. From the Figs. 4 - 18, obtained through simulations, one can observe that the i_{Lm} magnetizing current , is the most distorted with the third harmonic of 67.73% out of the magnitude of the fundamental harmonic, followed by the i_{As} stator current with its third harmonic at 39,01% out of its fundamental. For the rotor current ira the third harmonic is “only” 23.30% out of the magnitude of its fundamental.

Voltages across the three coils of the circuit are even more distorted because of the proportionality to the time derivatives of their correspondent currents. The third harmonic of the v_{Ls} voltage exceeds the magnitude of the fundamental (116.8%) and the harmonic of 5th order is 67.38 % out of the magnitude of its fundamental. On the other hand, the most significant harmonics of the v_L voltage waveform are of order 3, 5, 6, 7, 9, 11, 13 and 15. For v_{Lm} the third harmonic is equal to 23.91% out of the fundamental while the 7th harmonic exceeds with 2.28% out of the fundamental.

P_{Cu1} stator copper loss (Fig. 16) is the most affected by the saturation: 2.543 times larger in comparison to the linear magnetic core case, while the P_{RFe} core loss is slightly smaller (0.89556 times smaller in comparison to the linear magnetic core case, Fig. 18). When considering saturation, the electromagnetic torque (Fig. 20) increases 1.2387 times with respect to the non-saturated magnetic core.

4. CONCLUSIONS

In our paper is studied the saturation influence on the asynchronous motor performances. For this, starting from the equivalent scheme on a phase, when we take into account that the magnetization inductance is considered as the current-controlled nonlinear inductor and the rotor resistor as a time-variable resistor, it was analyzed the induction motor working in the steady-state behavior. The simulations were done by the dedicated performance programs (elaborated by the authors): ACAP – Analog Circuit Analysis Program, CSAP – Circuit Symbolic Analysis Program and, for to compare the results, by the SPICE program. All these programs are based on the modified nodal equations and they permit the Fourier analysis for all current and voltage waveforms. In this way we can compute any high order harmonics which appear in the time variations of these quantities. It was found out an excellent correspondence between the asynchronous motor ratings obtained through simulation with the catalog data.

When take into account saturation phenomenon, the phase current displays high order harmonics. An immediate consequence of the presence of these current harmonics was an increase in the losses and a decrease of the efficiency and the motor power factor in comparison to the non-saturated magnetic core assumption. The analysis of the saturation influence on asynchronous motors in steady-state behavior can also be done using the state equations which can integrate by one of the integration routines from the Toolbox MATLAB.

From the results obtained through simulations we could find the presence of a heavy content of harmonics in both voltage and current time varying waveforms. This fact explains the increase in terms of copper and core losses and decrease of the efficiency and the power factor. However, the developed (electromagnetic) torque increased significantly.

The originality of this paper stands in the fact that ACAP, SYSEG and CSAP can analyze analogue circuits in a completely symbolic, numeric - symbolic or numerical way which allows that certain parameters from the equivalent circuit of the asynchronous motor to be considered as symbols. This way analysis can be made, in different work regimes for the motor, for the work performances related to these parameters. In order to integrate the linear and/or nonlinear differential equations, MATLAB routines were used which are very efficient in solving this type of equations.

CONFIRMATION

The work was presented at *Electric machines, materials and drives* Symposium SME'XXI, edition 2025.

REFERENCES

1. L.O. Chua, P.M. Lin, *Computer-Aided analysis of electronic circuits: Algorithms and computational techniqu*es, Englewood cliffs, NJ: Prentice-Hall, 1975.
2. E. Schwarz, *Computer-aided design of microelectronic circuits and systems*, Academic Press, London, 1987.
3. M. Iordache, L. Dumitriu*, Computer-aided simulation of analog circuits – Algorithms and computational techniques*, POLITEHNICA Press Publishing House , Bucharest, 2014.
4. M. Iordache, S. Deleanu, C. Curteanu, N. Galan, A.A. Moscu, *SYSEG - SYmbolic State Equation Generation*, Proc. of the 11-th International Conference on Electromechanical and Power Systems, SIELEM, Chişinău Rep. MOLDOVA, IEEE, pp. 1-7, October 11-14, 2017
5. M. Stănculescu, A. Ionescu, D. Sanatescu, S. Deleanu, L. Bobaru, A.A. Moscu, *CSAP – Transfer Function SYmbolic Generation and TFSYG – Transfer Function SYmbolic Generation*, Proc. of the 12th International Conference on Electromechanical and Power Systems, SIELEM, Chişinău Rep. MOLDOVA, IEEE Xplore, Publisher: IEEE, pp. 1-7, October 10-11, 2019.
6. M. Iordache, H.S. Popescu, I. Vlad, M.F. Staniloiu, *ACAP – Analog Circuit Analysis Program*, Proceeding of the 12th International Symposium Advanced Topics in Electrical Engineering – ATEE'21, Editura Politehnica Press, pp. 373 - 377, IEEE Xplore, Publisher:IEEE, Bucharest, Romania March 25-27, 2021
7. C. Mihăilescu, Fl. Rezmeriţă, I. Calomfirescu, M. Iordache, N. Galan, *Performance analysis of three phase-squirred cage induction motor with deep rotor bars in transient behavio*r, Electrical and Electronic Engineering, **2**, *2*, pp. 11-17, 2012.
8. R. Voiculescu, I. Mihai, *Analog circuit simulation by state variable method*, U.P.B. Scientific Bulletin Series C – Electrical Engineering, **71**. *3*, pp. 213-224, 2015.
9. M. Iordache, N. Voicu, L. Dumitriu, C. Petrescu, *Steady-state thermal field analysis of the turbo-generator rotor with direct cooling*, Advanced Electrical and Computer Engineering, Academy of Technical Sciences of Romania „Stefan cel Mare", **7**, *14,* **2**, *28*, Web of Science pp. 28-32, 2007.
10. A.-K. Repo, P. Rasilo, A.A. Arkkio, *Dynamic electromagnetic torque model and parameter estimation for a deep-bar induction machine*, IET Electr. Power Appl., **2**, *3*, pp. 183 -192, 2008.
11. E. Levi*, Main flux saturation modelling in double-cage and deep-bar induction machines*, IEEE Trans. Energy Conversion, **11**, *2*, pp.305 – 311, 1996.
12. K.S. Huang, Q.H. Wu, D.R. Turner*, Effective identification of induction motor parameters based on fewer measurements*. IEEE Trans. Energy Converssion, **17**, *1*, pp.305 – 311, pp. 55 – 59, 2002.
13. J. Pedra, L Sainz, *Parameter estimation of squirrel-cage induction motors without torque measurements*, IEE Proc. Electr. Power Appl., **153**, *2,* pp. 87 -94, 2006.
14. Rik W.A.A. De Doncker, *Field-Oriented controllers with rotor deep bar compensation circuits*, IEEE Trans. Industry Applications, **28**, *5* , pp. 1062 – 1070, 1992.
15. Jul-Ki Seok, Seung-Ki Sul, *Pseudorotor-flux-oriented control of an induction machine for Deep-Bar-e ffect compensation*, IEEE TRANS. INDUSTRY APPLICATIONS, **34**, *3* , pp. 429 – 434 , 1998.
16. Alexander C. Smith, Russell C. Healez, Stephen Williamson, *A transient induction motor model including saturation and deep bar effect*, IEEE Trans. Energy Converssion, **11**, *1,* pp.8 -15, 1996.
17. L. Ljung, *System identification: Theory for the user, 2nd edition*, Prentice Hall, USA, 1999.
18. J. Pedra, F. Corcoles*, Estimation of induction motor double-cage model parameters from manufacturer data*, IEEE Transactions on Energy Conversion, June 2004.
19. T. Phumiphak, C. Chatuthai, *Estimation of induction motor parameters based on a field test coupled with genetic algorithm*, in Proc. Int. Conf. Power System Technology, pp. 1199-1203, 2002.